ELSEVIER

Journal of Fluids and Structures 19 (2004) 765–783

JOURNAL OF FLUIDS AND STRUCTURES

www.elsevier.nl/locate/jnlabr/yjfls

Limit-cycle stability reversal via singular perturbation and wing-flap flutter

D. Dessi[a], F. Mastroddi[b,*]

[a] *INSEAN, Via di Vallerano, 139, I-00128 Rome, Italy*

[b] *Dipartimento di Ingegneria Aerospaziale e Astronautica, Università degli Studi di Roma ''La Sapienza'', Via Eudossiana 18, I-00184 Rome, Italy*

Received 21 January 2003; accepted 18 April 2004

Abstract

A three-degree-of-freedom aeroelastic typical section with a trailing-edge control surface is theoretically modelled, including nonlinear springs for both the nonlinear description of the torsional stiffness and of the hinge elastic moment. Furthermore, augmented states for linear unsteady aerodynamic of 2-D incompressible potential flow, have been considered in the model. First, the system response is determined by numerically integrating the governing equations using a standard Runge–Kutta algorithm in conjunction with a 'shooting method'. The numerical analysis has revealed the presence of stable and unstable limit cycles, along with stability reversal in the neighborhood of a Hopf bifurcation. Consequently, the equations of motion are analysed by a singular perturbation technique based on the normal-form method. This method, originally introduced by strictly applying a resonance condition, is herein extended by applying a near-resonance condition in order to improve the semi-analytical description of the stability reversal behavior. Therefore, amplitudes and frequencies of limit cycles depending on the flow speed V are obtained from the normal-form equations, and the terms which are essentially responsible for the nonlinear system behavior are identified.

1. Introduction

The prediction of the speed above which the system becomes unstable is one of the most relevant objectives in studying linear and nonlinear fixed-wing aeroelasticity. If the instability involves oscillations, the phenomenon is called flutter, otherwise it is called divergence. According to linear stability analysis, the oscillations beyond the so-called (linear) flutter speed V_F are not damped and their amplitude grows indefinitely, from a mathematical point of view, leading to the collapse of the wing structure. In the case of nonlinear aeroelastic systems, more attention must be paid to the effects that some kinds of nonlinearities may induce on flutter. In Dowell et al. (1997) an exhaustive review of the scenario of nonlinear aeroelastic phenomena has been presented. Within this framework, nonlinear torsional stiffness and control-surface freeplay have a relevant role, as one can see in the technical literature over the last decade; like in Lee and Tron (1989), Alighanbari and Price (1996), Lee et al. (1997), Lacabanne (1997), Conner et al. (1997), Lee et al. (1998). In these papers the nonlinear aeroelastic vibration of a 2-degree of freedom (2-dof) pitching and plunging airfoil or 3-degree of freedom (3-dof) pitching, plunging airfoil with a control-surface-independent rotation with structural freeplay nonlinearities have been numerically studied and sometimes compared with experimental results. Indeed, these kinds of nonlinear aeroelastic models are typically considered as tools by the researchers, both to validate the used physical simplified model by means of comparison with experimental results and, above all, to validate numerical and

*Corresponding author. Tel.: +39-6-44585945; fax: +39-6-4458-5670.

E-mail addresses: d.dessi@insean.it (D. Dessi), franco.mastroddi@uniroma1.it (F. Mastroddi).

0889-9746/$ - see front matter © 2004 Elsevier Ltd. All rights reserved.
doi:10.1016/j.jfluidstructs.2004.04.010

analytical methodology to study aeroelastic systems; also significant in this case is the use for this nonlinear aeroelastic model of signal-processing theory, by means of an input/output system analysis, to identify the nonlinear behavior of the system, as shown in Mastroddi and Bettoli (1999) and Alighanbari and Lee (2003).

Focusing attention on this nonlinear aeroelastic system when exhibiting limit-cycle oscillations (LCO), the nonlinear-flutter behavior may be classified into two types: benign and explosive flutter. In the first case, above the linear flutter speed, the system tends to stable limit-cycle oscillations (LCOs), leading to a supercritical Hopf bifurcation; whereas in the second case, even below the linear flutter speed, the system, for small values of $V_F - V$, may experience instability, provided that the initial conditions are sufficiently high, namely a subcritical Hopf bifurcation. From a practical point of view, the second case (known as 'explosive' or 'destructive' flutter, see Fig. 1), implies that below the linear flutter speed V_F (as obtained from the linear analysis) the system experiences a sudden onset of a destructive instability. However, an even more frightening implication is that the linear flutter speed is not at all a safe prediction, since this destructive instability may occur even below the linear flutter speed V_F, provided that the wing experiences a sufficiently high perturbation as, for example, an encountered gust. It should be emphasized that such an analysis is not used in the actual design of aircraft.

However, there is well-known experimental evidence, e.g., in Lacabanne (1997), Chen et al. (1998) and Matsushita et al. (2001), as well as numerical evidence as shown in Woolston et al. (1957), Lee et al. (2002) and Dessi et al. (2002), that a combination of (i) small-amplitude unstable limit cycles, and (ii) large-amplitudes stable limit cycles may occur below the linear flutter speed, i.e., the possibility, under suitable initial conditions, of *finite*-amplitude LCOs below the linear flutter speed. This phenomenon is depicted in Fig. 2, which shows a subcritical Hopf bifurcation exhibiting a so-called turning point [Nayfeh and Balachandran (1994)] at a velocity lower than the (linear) flutter speed, determining a 'knee' in the bifurcation diagram where the unstable limit-cycle (sub-critical Hopf bifurcation) reverses into a stable

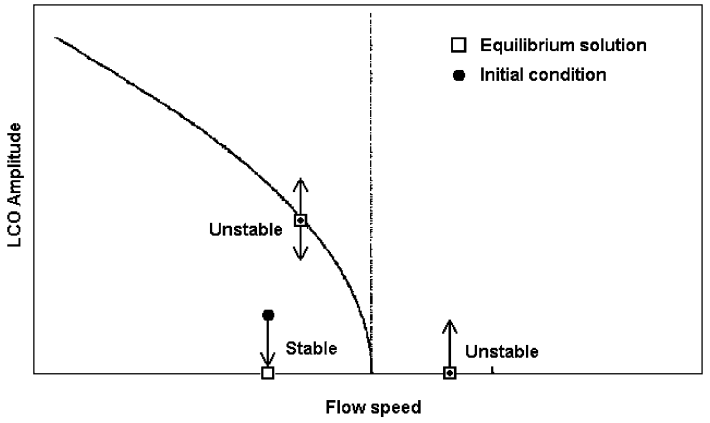

Fig. 1. Hopf bifurcation of pitchfork-like shape.

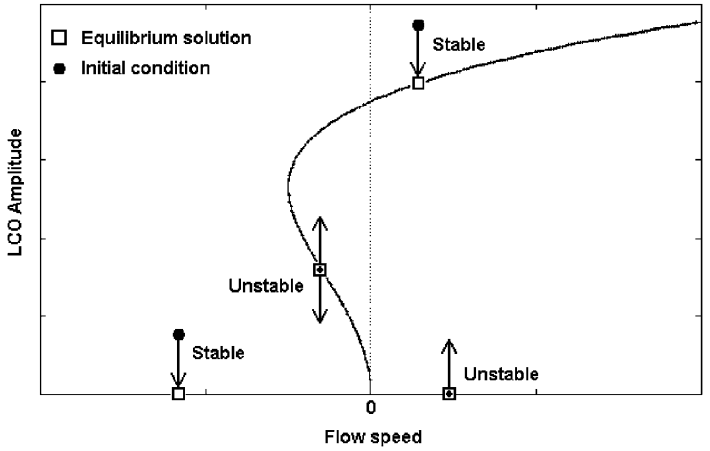

Fig. 2. Hopf bifurcation of knee-like shape.

one. For instance, in Dessi et al. (2002) it has been underlined how a proper choice of some structural parameter in a 2-dof typical section model with a nonlinear spring (e.g., the distance between the aerodynamic center and the elastic center) can determine the bifurcation type (e.g., limit-cycle stability and reversal) in the neighborhood of the linear flutter speed V_F.

In this paper both the standard LCO analysis in the neighborhood of the flutter speed and the higher-order analysis, (i.e., LCO stability reversal at the turning point) have been applied to a 3-dof aeroelastic system. Furthermore, the results obtained via numerical simulation have been compared with those given by using a perturbation technique; specifically, the normal-form (NF) method has been applied for this purpose. As a natural consequence, the semi-analytic procedure associated with the NF analysis has allowed the identification of the nonlinear contributions responsible in the mathematical model for the reversal behavior. The main features of the bifurcation diagrams—critical point (linear flutter speed), turning point abscissa (minimum speed for undamped oscillations) and related amplitudes—have been studied with respect to some aeroelastic parameters characterizing a 2-D airfoil with a trailing-edge (TE) control surface.

The mathematical model for the 2-D airfoil aeroelasticity study, with a TE control surface, with nonlinear springs, is presented in Section 2. Next, in Section 3, the standard NF approach is briefly described. Finally, in Section 4, some results on different numerical simulations obtained with numerical integration and the NF singular perturbation technique are shown.

2. Equations of motion

Consider a 3-dof airfoil, elastically supported by a linear plunge spring and a nonlinear torsional spring. It is equipped with a control surface (flap) constrained to the wing with a nonlinear torsional spring (see Fig. 3). Using standard notation, the plunging deflection is denoted by h, positive in the downward direction, α is the pitch angle about the elastic axis, positive with nose up, and β is the flap angle, positive when the TE surface is moved down.

The elastic axis is located at a distance $a_h b$ from the mid-chord, where b is half the chord, while the wing mass center is located at a distance $x_\alpha b$ from the elastic axis. The axis of rotation for the flap is located at a distance $b_h b$ from the mid-chord, while the flap mass center is located at a distance $x_\beta b$ from the flap hinge. All the previous distances are positive when measured towards the TE of the airfoil.

The aeroelastic equations of motion for the linear model are as originally found in Theodorsen (1935). The extension of the typical-section equations to the case of nonlinear torsional springs can easily be achieved as in the following (see the appendix for details):

$$\begin{aligned}
&\ddot{\xi} + x_\alpha \ddot{\alpha} + x_\beta \ddot{\beta} + \frac{\Omega_1^2}{U^2}\xi = p,\\
&\frac{x_\alpha}{r_\alpha^2}\ddot{\xi} + \ddot{\alpha} + [r_\beta^2 + (b_h - a_h)x_\beta]\frac{1}{r_\alpha^2}\ddot{\beta} + \frac{1}{U^2}M_\alpha(\alpha) = r,\\
&\frac{x_\beta}{r_\beta^2}\ddot{\xi} + \left[1 + (b_h - a_h)\frac{x_\beta}{r_\beta^2}\right] + \ddot{\beta} + \frac{\Omega_2^2}{U^2}M_\beta(\beta) = s,
\end{aligned} \tag{1}$$

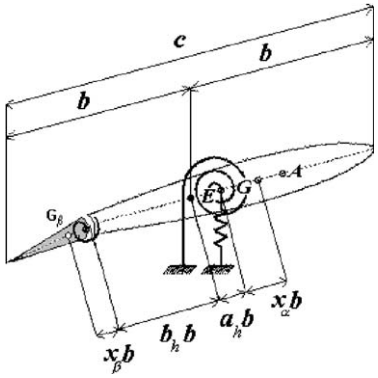

Fig. 3. Three-degree-of-freedom model of a typical section with control surface.

where the overdot denotes differentiation with respect to the nondimensional time τ, defined as $\tau = V\,t/b$, $\xi = h/b$ is the nondimensional plunge displacement of the elastic axis, $r_\alpha = \sqrt{J_\alpha/mb^2}$ is the reduced radius of gyration about the elastic axis, $r_\beta = \sqrt{J_\beta/mb^2}$ is the reduced radius of gyration about the flap hinge, $\mu = \pi\rho b^2/m$ is the mass ratio; note that $M_\alpha(\alpha)$ represents the overall contribution of the torsional spring moment of the wing section, while $M_\beta(\beta)$ represents the torsional spring moment of the flap, both including the linear and nonlinear part, respectively. Furthermore, Ω_1 and Ω_2 are given by $\Omega_1 = \omega_\xi/\omega_\alpha$ and $\Omega_2 = \omega_\beta/\omega_\alpha$, where ω_ξ, ω_α and ω_β are the uncoupled plunging, pitching and flapping natural frequencies, respectively; U is defined as $U = V/b\omega_\alpha$, where V is the dimensional speed. Moreover, p and r are, respectively, the lift and pitch aerodynamic moment for the wing, whereas s is the pitching moment acting on the flap. For incompressible two-dimensional flow, by combining the analytical expressions of the forces in the frequency domain given by Theodorsen (1935) with the expressions given in Fung (1955) in the time domain for plunge/pitch typical section, one obtains

$$
\begin{aligned}
p &= -\frac{1}{\mu}[\dot{\alpha} + \ddot{\xi} - a_h\ddot{\alpha} - (T_4/\pi)\dot{\beta} - (T_1/\pi)\ddot{\beta} - 2u(w_{3/4})],\\
r &= -\frac{1}{\mu r_\alpha^2}[\bar{a}_h\dot{\alpha} + (1/8 + a_h^2)\ddot{\alpha} - a_h\ddot{\xi} + (T_4/\pi + T_{10}/\pi)\beta + (T_1/\pi - T_8/\pi - (b_h - a_h)T_4/\pi + 1/2(T_{11}/\pi))\dot{\beta}\\
&\quad - (T_7/\pi + (b_h - a_h)T_1/\pi)\ddot{\beta} - 2u(w_{3/4})],\\
s &= -\frac{1}{\mu r_\beta^2}[(-2T_9/\pi - T_1/\pi - \bar{a}_h T_4/\pi)\dot{\alpha} + 2(T_{13}/\pi)\ddot{\alpha} + (T_5/\pi^2 - T_4T_{10}/\pi^2)\beta - 1/2(T_4/\pi)(T_{11}/\pi)\dot{\beta} - (T_3/\pi^2)\ddot{\beta}\\
&\quad - (T_1/\pi)\ddot{\xi} + (T_{12}/\pi)u(w_{3/4})],
\end{aligned}
\tag{2}
$$

where the circulatory part of the lift and pitching moments denoted by $u(w_{3/4})$ in the above expressions is given, in the case of zero initial conditions, by

$$
u(w_{3/4}) = \int_0^\tau \phi(\tau - \sigma)\dot{w}_{3/4}(\sigma)\,\mathrm{d}\sigma \tag{3}
$$

with $w_{3/4}(\tau) = \dot{\xi}(\tau) + \bar{a}_h\dot{\alpha}(\tau) + \alpha(\tau) + (T_{10}/\pi)\dot{\beta} + (T_{11}/2\pi)\ddot{\beta}$, $\bar{a}_h = 1/2(1 - a_h)$, and $\phi(t)$ being the Wagner function [see Theodorsen (1935) for the definition of T_is]. Using the classical finite-state approximation for the Wagner function ϕ introduced in Jones (1940) [see also [Edwards et al. (1979)] for an equivalent procedure in the Laplace domain], the problem may be recast (Dessi et al., 2002) as a system of eight first-order differential equations,

$$
\dot{\mathbf{w}} = \mathbf{A}(U)\mathbf{w} + \mathbf{r}(\mathbf{w}, U), \tag{4}
$$

where $\mathbf{w} = \{\dot{\xi}, \dot{\alpha}, \dot{\beta}, \dot{u}, \xi, \alpha, \beta, u\}^{\mathrm{T}}$ is the state-space vector, $\mathbf{A}(U)$ is the linear part of the equations of motion as obtained by Eqs. (1) and (2) and $\mathbf{r}(\mathbf{w}, U)$ is the vector of nonlinear terms.

Using the linear coordinate transformation $\mathbf{w} = \mathbf{R}\mathbf{z}$ induced by the local eigenproblem $\mathbf{A}(U_F)\mathbf{R} = \mathbf{R}\mathbf{\Lambda}$, the following linearly diagonal format is obtained:

$$
\dot{\mathbf{z}} = \mathbf{\Lambda}\mathbf{z} + \mathbf{f}(\mathbf{z}, U), \tag{5}
$$

which is the starting point for the application of the NF technique.

It is worth pointing out that, from a modelling point of view, Eq. (4) is quite representative of an aeroelastic system exhibiting a nonlinear behavior in the sense that, e.g., its linear portion can be described with standard commercial codes. Indeed, by using a modal description for the structures and a finite-state representation for the aerodynamics (Morino et al. 1995), the displacements with respect to an equilibrium solution (i.e., the fixed-wing trim conditions) at given locations and the unsteady loads have to be determined. Thus, introducing a set of N generalized coordinates, and $N + M$ additional states composed by the N first time derivatives of the generalized coordinates and the M aerodynamic states, the state space vector can be written in this general case as

$$
\mathbf{w}^{\mathrm{T}} = \{q_1, q_2, \ldots, q_N, q_{N+1}, q_{N+2}, \ldots, q_{2N+M}\}. \tag{6}
$$

3. Normal-form analysis

In this section the essentials of the normal-form (NF) method applied for the nonlinear analysis of higher-order Hopf bifurcations is presented. It is a general singular perturbation technique, based on the idea that a nonlinear system can be simplified by a suitable transformation of the state-space variables in the phase space. This goal is achieved by two

different steps: by reducing the number of equations and by using the NF method to eliminate in the reduced equations the nonlinear terms that do not contribute significantly to the solution. For both steps, the selection of the linear and nonlinear terms is performed by introducing the so-called "near-resonance condition" (Dessi et al., 2002). Next, the methodology is presented, for the limited case of algebraic nonlinearities.

Consider a one-parameter system of N nonlinear differential equations

$$\dot{x}_n = \mathscr{H}_n(x_1, x_2, \ldots, x_n, \ldots, x_N; \mu), \quad n = 1, \ldots, N, \tag{7}$$

with N unknowns, and we assume that $\mathscr{H}_n(x_1, \ldots, x_N; \mu)$ be an analytic function (in particular a polynomial) of the variables $x_1, \ldots, x_N$ and the parameter μ.

There are two ways of dealing with the system parameter μ: (i) adding a supplementary equation $\dot{\mu} = 0$ to Eq. (7), or (ii) using a rescaling parameter ε to provide an expansion for μ. In the first case, the parameter μ is considered like a state-space variable and the NF-method has to be applied to the "augmented system" of $N + 1$ equations; this generally simplifies the numerical implementation of the NF technique. In the second case, the cascade of equations obtained is ordered with respect to the rescaling parameter ε (which has to be eliminated to turn back to the original variables) and not, as in the first case, with respect to a norm of the unknown; nevertheless, this version of the NF method seems to be more intuitive and it will be preferred in the following. Note that, for the present problem, no practical difference in the numerical results can be detected between the two versions of the NF method.

Taking a Taylor expansion of $\mathscr{H}_n(\mathbf{x}; \mu)$ around $x_n = 0$ with $n = 1, \ldots, N$ and assuming $\mathscr{H}_n(\mathbf{0}; \mu) = \mathbf{0}$, the dynamical system may be re-written as

$$\dot{x}_n = \hat{A}_{np}(\mu)x_n + \sum_{p,q=1}^{N} \hat{b}_{npq}(\mu)x_p x_q + \sum_{p,q,r=1}^{N} \hat{c}_{npqr}(\mu)x_p x_q x_r + \cdots . \tag{8}$$

For the sake of conciseness in outlining the NF method applied to higher-order Hopf bifurcations, it is convenient to re-write the previous equation using the vector notation

$$\dot{\mathbf{x}} = \hat{\mathbf{A}}(\mu)\mathbf{x} + \hat{\mathbf{b}}(\mathbf{x}, \mathbf{x}; \mu) + \hat{\mathbf{c}}(\mathbf{x}, \mathbf{x}, \mathbf{x}; \mu) + \mathscr{O}(\|\mathbf{x}\|^4), \tag{9}$$

where $\hat{\mathbf{A}}$ is an $N \times N$ matrix, whereas $\hat{\mathbf{b}}$ and $\hat{\mathbf{c}}$ are a bilinear and a trilinear form, respectively.

Let $\hat{\lambda}_i(\mu)$ denote the eigenvalues of $\hat{\mathbf{A}}(\mu)$. In the following, we assume that for a given value of μ (which, without loss of generality, we assume to be zero) the system becomes unstable. Specifically, we set $\lambda_i = \hat{\lambda}_i(0)$.

Moreover, we assume also that $\lambda_1 = \bar{\lambda}_2 = \mathrm{i}\omega$ and that $\mathrm{Real}[\lambda_i] < 0$ for $i = 3, \ldots, N$. In addition, we assume that in the positive neighborhood of $\mu = 0$, $\hat{\lambda}_1^R = \mathrm{Real}[\hat{\lambda}_1] > 0$ and that $\mathrm{Real}[\hat{\lambda}_i] < 0$ $(i = 3, \ldots, N)$.

On the basis of the above assumptions, we can write

$$\hat{\mathbf{A}} = \hat{\mathbf{A}}_0 + \mu\hat{\mathbf{A}}_1 + \mathscr{O}(\mu^2). \tag{10}$$

Next, we also assume that λ_j eigenvalues of the matrix $\hat{\mathbf{A}}_0$ are distinct. Hence, $\hat{\mathbf{A}}_0$ will have linearly independent right eigenvectors $\mathbf{r}_i$, with $\mathbf{R} = [\mathbf{r}_1, \mathbf{r}_2, \ldots, \mathbf{r}_N]$ such that

$$\mathbf{R}^{-1}\hat{\mathbf{A}}_0\mathbf{R} = \mathbf{\Lambda}, \tag{11}$$

where $\mathbf{\Lambda} = \mathrm{diag}(\lambda_1, \ldots, \lambda_N)$ is diagonal matrix with elements equal to $\lambda_1, \ldots, \lambda_N$.

Then, setting $\mathbf{x} = \mathbf{R}\mathbf{z}$ and pre-multiplying Eq. (9) by $\mathbf{R}^{-1}$, one has

$$\dot{\mathbf{z}} = (\mathbf{\Lambda} + \mu\mathbf{A}_1)\mathbf{z} + \mathbf{b}(\mathbf{z}, \mathbf{z}) + \mathbf{c}(\mathbf{z}, \mathbf{z}, \mathbf{z}) + \mathscr{O}(\|\mathbf{z}\|^3) + \mathscr{O}(\mu^2) + \mathscr{O}(\mu\|\mathbf{z}\|^2),$$

where $\mathbf{A}_1 = \mathbf{R}^{-1}\hat{\mathbf{A}}_1\mathbf{R}$, $\mathbf{b}(\mathbf{z}, \mathbf{z}) = \mathbf{R}^{-1}\hat{\mathbf{b}}(\mathbf{R}\mathbf{z}, \mathbf{R}\mathbf{z}; 0)$, and $\mathbf{c}(\mathbf{z}, \mathbf{z}, \mathbf{z}) = \mathbf{R}^{-1}\hat{\mathbf{c}}(\mathbf{R}\mathbf{z}, \mathbf{R}\mathbf{z}, \mathbf{R}\mathbf{z}; 0)$. Next, we introduce the ordering parameter ε such that $\mathbf{z} = \varepsilon\mathbf{u}$. Note that the introduction of this new state-space variable which is a typical issue in perturbation methods (Nayfeh and Balachandran (1994)) allows one to scale the contributions of any terms in each equations on the base of the amplitude of the original state-space variable $\mathbf{z}$. Hence,

$$\dot{\mathbf{u}} = \mathbf{\Lambda}\mathbf{u} + \mu\mathbf{A}_1\mathbf{u} + \varepsilon\mathbf{b}(\mathbf{u}, \mathbf{u}) + \varepsilon^2\mathbf{c}(\mathbf{u}, \mathbf{u}, \mathbf{u}) + \mathscr{O}(\varepsilon^3) + \mathscr{O}(\mu^2) + \mathscr{O}(\mu\varepsilon). \tag{12}$$

For simplicity, in this work we can assume that the even nonlinear terms vanish (this is true because the system is symmetric, so that the equations are invariant if $\mathbf{u}$ is replaced by $-\mathbf{u}$). Then, we have

$$\dot{\mathbf{u}} = \mathbf{\Lambda}\mathbf{u} + \mu\mathbf{A}_1\mathbf{u} + \varepsilon^2\mathbf{c}(\mathbf{u}, \mathbf{u}, \mathbf{u}) + \mathscr{O}(\varepsilon^4) + \mathscr{O}(\mu^2) + \mathscr{O}(\mu\varepsilon^2), \tag{13}$$

since the even terms in $\mathbf{u}$ (in particular, the fourth-order terms) have been assumed to vanish. Finally, in order to balance the nonlinear terms with the increase in the linear terms, $\mu\mathbf{A}_1\mathbf{u}$ (this will be clearer later), we choose

$$\mu = \pm\varepsilon^2. \tag{14}$$

Then, we have

$$\dot{\mathbf{u}} = \mathbf{\Lambda u} + \varepsilon^2[\mathbf{Au} + \mathbf{c}(\mathbf{u},\mathbf{u},\mathbf{u})] + \mathcal{O}(\varepsilon^4) \tag{15}$$

with $\mathbf{A} = \pm\mathbf{A}_1$.

The above problem may be written as

$$\dot{\mathbf{u}} = \mathbf{\Lambda u} + \varepsilon^2\mathbf{f}^{(2)}(\mathbf{u}) + \mathcal{O}(\varepsilon^4) \tag{16}$$

with $\mathbf{f}^{(2)}(\mathbf{u}) = \mathbf{Au} + \mathbf{c}(\mathbf{u},\mathbf{u},\mathbf{u})$. The normal-form method consists of simplifying the differential problem through the "near-identity" coordinate transformation

$$\mathbf{u} = \mathbf{y} + \varepsilon^2\mathbf{w}^{(2)}(\mathbf{y}) + \mathcal{O}(\varepsilon^4), \tag{17}$$

where $\mathbf{w}^{(2)}(\mathbf{y})$ is to be chosen so as to simplify the problem. Combining Eqs. (16) and (17) one obtains

$$\dot{\mathbf{u}} = \dot{\mathbf{y}} + \varepsilon^2\mathbf{W}\dot{\mathbf{y}} + \mathcal{O}(\varepsilon^4) = \mathbf{\Lambda}(\mathbf{y} + \varepsilon^2\mathbf{w}^{(2)}(\mathbf{y})) + \varepsilon^2\mathbf{f}^{(2)}(\mathbf{y} + \cdots) + \mathcal{O}(\varepsilon^4), \tag{18}$$

where $\mathbf{W} = \partial\mathbf{w}^{(2)}/\partial\mathbf{y}$, or, using $(\mathbf{I} + \varepsilon^2\mathbf{W})^{-1} = \mathbf{I} - \varepsilon^2\mathbf{W} + \mathcal{O}(\varepsilon^4)$,

$$\dot{\mathbf{y}} = (\mathbf{I} - \varepsilon^2\mathbf{W})[\mathbf{\Lambda}(\mathbf{y} + \varepsilon^2\mathbf{w}^{(2)}(\mathbf{y})) + \varepsilon^2\mathbf{f}^{(2)}(\mathbf{y})] + \mathcal{O}(\varepsilon^4). \tag{19}$$

Collecting same-order terms yields

$$\dot{\mathbf{y}} = \mathbf{\Lambda y} + \varepsilon^2\mathbf{g}^{(2)}(\mathbf{y}) + \mathcal{O}(\varepsilon^4), \tag{20}$$

where

$$\mathbf{g}^{(2)}(\mathbf{y}) = -\mathbf{W\Lambda y} + \mathbf{\Lambda}\mathbf{w}^{(2)}(\mathbf{y}) + \mathbf{f}^{(2)}(\mathbf{y}). \tag{21}$$

Eq. (20) is formally equal to Eq. (16) although the vector field $\mathbf{w}^{(2)}(\mathbf{y})$ (and its derivative) has to be defined in order to simplify the transformed problem given by Eq. (20). Next, we choose $\mathbf{w}^{(2)}(\mathbf{y})$ so as to remove all the terms that cause unnecessary complexity in Eq. (16). To be specific, using the indicial notations, $\mathbf{f}^{(2)}(\mathbf{y}) = \mathbf{Ay} + \mathbf{c}(\mathbf{y},\mathbf{y},\mathbf{y})$ may be written as

$$f_n^{(2)}(y_k) = \sum a_{np}y_p + \sum c_{npqr}y_py_qy_r. \tag{22}$$

Thus, the objective of choosing Eq. (17) so as to render Eq. (20) simpler than Eq. (16), is achieved by choosing for $\mathbf{w}^{(2)}(\mathbf{y})$ to have the same functional dependence as Eq. (22), i.e.,

$$w_n^{(2)}(y_k) = \sum \alpha_{np}y_p + \sum \gamma_{npqr}y_py_qy_r, \tag{23}$$

where α_{np} and γ_{npqr} are to be determined (see later). This implies

$$w_{n,k}^{(2)} = \frac{\partial w_n^{(2)}}{\partial y_k} = \sum \alpha_{np}\delta_{pk} + \sum \gamma_{npqr}(\delta_{pk}y_qy_r + y_p\delta_{qk}y_r + y_py_q\delta_{rk}). \tag{24}$$

Combining Eqs. (21), (22) and (24), one obtains

$$\begin{aligned} g_n^{(2)}(y_k) &= \sum w_{n,p}^{(2)}\lambda_p y_p + \lambda_n w_n^{(2)}(y_k) + f_n(y_k) \\ &= -\sum \alpha_{np}\lambda_p y_p - \sum \gamma_{npqr}(\lambda_p + \lambda_q + \lambda_r)y_py_qy_r + \lambda_n\left(\sum \alpha_{np}y_p + \sum \gamma_{npqr}y_py_qy_r\right) \\ &\quad + \sum\left(a_{np}y_p + \sum c_{npqr}y_py_qy_r\right) \\ &= \sum [a_{np} - (\lambda_p - \lambda_n)\alpha_{np}]y_p + \sum [c_{npqr} - (\lambda_p + \lambda_q + \lambda_r - \lambda_n)\gamma_{npqr}]y_py_qy_r. \end{aligned} \tag{25}$$

Next, we choose α_{np} and γ_{npqr} so as to eliminate from the term given by Eq. (25) as many terms as possible. Specifically, this objective may be achieved if one sets

$$\alpha_{np} = \begin{cases} \dfrac{a_{np}}{\lambda_p - \lambda_n} & \text{if } \lambda_p - \lambda_n \neq 0, \\ 0 & \text{otherwise;} \end{cases} \tag{26}$$

$$\gamma_{npqr} = \begin{cases} \dfrac{c_{npqr}}{\lambda_p + \lambda_q + \lambda_r - \lambda_n} & \text{if } \lambda_p + \lambda_q + \lambda_r - \lambda_n \neq 0, \\ 0 & \text{otherwise.} \end{cases} \tag{27}$$

These equations, combined with Eq. (23), define completely the vector $\mathbf{w}^{(2)}(\mathbf{y})$. Thus, one can go back to the "transformed problem" given by Eq. (20), where $\mathbf{g}^{(2)}(y_k)$ is now given by

$$g_n^{(2)}(y_k) = \sum_{p \in I_p^n} a_{np} y_p + \sum_{pqr \in I_{pqr}^n} c_{npqr} y_p y_q y_r, \tag{28}$$

where, according to Eqs. (26) and (27) I_p^n and I_{pqr}^n are given by

$$I_p^n = \{(n;p) | \lambda_p = \lambda_n\}, \tag{29}$$

$$I_{pqr}^n = \{(n;p,q,r) | \lambda_p + \lambda_q + \lambda_r = \lambda_n\}. \tag{30}$$

Eq. (20), with $\mathbf{g}^{(2)}(\mathbf{y})$ given by Eqs. (28)–(30), is indeed simpler to solve then Eq. (16).

It is important to remark that, in the case of dynamical systems exhibiting higher-order Hopf bifurcations, also the fourth-order terms have to be analysed because they may significantly contribute to the solution. This is the case of the aeroelastic system considered in this paper, where the fourth-order terms were not present in Eq. (16) but they are generated by the second-order normal-form procedure (this statement can be demonstrated by recasting Eq. (4) in the form of Eq. (8) and assuming cubic nonlinearities). Therefore, considering Eq. (20) and considering the fourth-order terms, the following equation needs to be simplified by the NF procedure:

$$\dot{\mathbf{y}} = \mathbf{\Lambda} \mathbf{y} + \varepsilon^2 \mathbf{g}^{(2)}(\mathbf{y}) + \varepsilon^4 \mathbf{f}^{(4)}(\mathbf{y}) + \mathcal{O}(\varepsilon^6). \tag{31}$$

Again, the NF-method consists of searching for a new state-space coordinates through the "near-identity" transformation

$$\mathbf{y} = \mathbf{v} + \varepsilon^4 \mathbf{w}^{(4)}(\mathbf{v}) + \mathcal{O}(\varepsilon^6), \tag{32}$$

where $\mathbf{w}^{(4)}(\mathbf{y})$ is to be chosen so as to simplify Eq. (31). The transformed dynamical system will be in the form

$$\dot{\mathbf{v}} = \mathbf{\Lambda} \mathbf{v} + \varepsilon^2 \mathbf{g}^{(2)}(\mathbf{v}) + \varepsilon^4 \mathbf{g}^{(4)}(\mathbf{v}) + \mathcal{O}(\varepsilon^6). \tag{33}$$

The procedure to determine both the unknown coordinate transformation $\mathbf{w}^{(4)}(\mathbf{v})$ and the resonant terms $\mathbf{g}^{(4)}(\mathbf{v})$ is formally identical to those outlined for the second-order terms (Eqs. (22)–(30)).

For Hopf bifurcation analysed in the frame of the Center Manifold theorem, Eq. (33) in the unknown $\mathbf{v}$ (the so-called "resonant" equation) will include as significant only scalar equations corresponding to the critical eigenvalues $\lambda_1 = \bar{\lambda}_1 = \mathrm{i}\omega$; this implies, by using trivially the coordinate transformation $\mathbf{u} = \mathbf{y} = \mathbf{v}$ (higher-order terms can be disregarded in Eqs. (14), (17) and (32)), that the relevant part of the nonlinear dynamics of the system will be given by the "manifold" associated to the pair of complex conjugate equations

$$\begin{aligned}
\dot{u}_1 &= \lambda_1 u_1 + \mu \sum_{p \in I_p^1} a_{1p} u_p + \sum_{pqr \in I_{pqr}^1} c_{1pqr} u_p u_q u_r + \sum_{pqrst \in I_{pqrst}^1} e_{1pqrst} u_p u_q u_r u_s u_t, \\
\dot{u}_2 &= \lambda_2 u_2 + \mu \sum_{p \in I_p^2} a_{2p} u_p + \sum_{pqr \in I_{pqr}^2} c_{2pqr} u_p u_q u_r + \sum_{pqrst \in I_{pqrst}^2} e_{2pqrst} u_p u_q u_r u_s u_t,
\end{aligned} \tag{34}$$

where $e_{1pqrst} = \bar{e}_{2pqrst}$ is the generic coefficient of the fifth-order monomial in the variable u_k.

$$I_{pqrst}^n = \{(n;p,q,r,s,t) | \lambda_p + \lambda_q + \lambda_r + \lambda_s + \lambda_t = \lambda_n\}. \tag{35}$$

However, it may happen that the center manifold hypothesis is violated, i.e., the manifold embedding the solution requires more coordinates $u_{i_1}, u_{i_2}, \ldots$ to be satisfactorily described (this point will be illustrated for higher-order Hopf bifurcations investigated in the following section). In other words, this implies that the coordinates $u_{i_1}, u_{i_2}, \ldots$ (associated to the damped eigenvalues) contribute significantly to the solution.

In this case, the natural way to improve the accuracy of the solution could be to consider more equations than those indicated by the Center Manifold theorem and to apply the zero resonant condition (as in Eqs. (26) and (27)) to retain the nonlinear terms in the transformed problem in the state-space variable $\mathbf{v}$. This procedure, however, might be inconsistent and, therefore, it is necessary also to loosen the zero-resonant condition stated in standard NF analysis, introducing a more appropriate 'near-resonant' condition (Dessi et al., 2002). It means that Eqs. (26)–(27) are replaced by the following inequality conditions:

$$\alpha_{np} = \begin{cases} \dfrac{a_{np}}{\lambda_p - \lambda_n} & \text{if } \|\lambda_p - \lambda_n\| \leqslant \rho, \\ 0 & \text{otherwise,} \end{cases} \tag{36}$$

$$\gamma_{npqr} = \begin{cases} \dfrac{c_{npqr}}{\lambda_p + \lambda_q + \lambda_r - \lambda_n} & \text{if } \|\lambda_p + \lambda_q + \lambda_r - \lambda_n\| \leqslant \rho, \\ 0 & \text{otherwise,} \end{cases} \tag{37}$$

where $\|.\|$ is the Euclidean norm, ρ is a small arbitrary positive real number such that as it becomes larger, more terms are retained in Eq. (34).

A geometrical interpretation of how the terms are chosen in the resonant equation is given in the following way. There is a one-to-one correspondence between terms in Eqs. (20) (or Eq. (33)) and the following complex quantities

$$\hat{\lambda}(i, j_1, \ldots, j_m) \coloneqq \lambda_i - (\lambda_{j_1} + \lambda_{j_2} + \ldots + \lambda_{j_m}) \ldots \tag{38}$$

denoted as $\hat{\lambda}$-points. Plotting all $\hat{\lambda}$-points in the complex plane corresponding to non-vanishing terms, the condition $\|.\| \leqslant \rho$ indicates that only the terms located inside a circle of radius ρ are retained in Eqs. (20) and (33). At this point, the smallest value of ρ, say ρ^*, that provides a good approximation for the solution of Eq. (16) has to be determined. This 'optimum' value of ρ exists by considering the two opposite limiting cases: (i) for $\rho = 0$ a pair of complex conjugate resonant equation with nonlinear terms up to the fifth order are obtained; (ii) for ρ arbitrarily large, all the equations with all the original cubic nonlinear terms are included (this is equivalent to a trivial diagonalization procedure of Eq. (7)).

An optimum $\rho^* \in (0, \infty)$ is provided in this paper as illustrated in the next section by a trial and error procedure.

4. Numerical results

In this section, the above formulation is applied to study the stability of the 3-dof typical section defined by Eq. (1) in the neighborhood of the linear flutter speed U_F. As mentioned before, all the analysis shown herein has been performed on the aeroelastic equations recast in the form of Eq. (4). In order to validate the procedure by which the first-order form of the aeroelastic equations was obtained, a linear stability analysis has been successfully performed on the typical section considered in Edwards et al. (1979), obtaining the same flutter speed. Next, a nonlinear model has been considered, assuming the pitching moment given by a cubic function $M_\alpha(\alpha) = c_{1\alpha}\alpha + c_{3\alpha}\alpha^3$, as in Alighanbari and Price (1996), and $M_\beta(\beta) = \beta$. The values of the coefficients considered in this case are $\mu = 100$, $x_\alpha = 0.25$, $\Omega_1 = 1.2$, $r_\alpha = 0.5$, $x_\beta = 0.0125$, $\Omega_2 = 3.5$, $r_\beta = 0.0791$, $b_h = 0.6$, whereas a_h assumes different values in several simulations.

The flutter speed and frequency are obtained by a linear standard eigenanalysis (Fig. 4; the poles are normalized with respect to ω_α for sake of clarity). In the case of $a_h = -0.5$, one obtains $U_F = 4.6724$ and $\omega_F = 0.268$; (note that the corresponding values for the same typical section without flap are $U_F = 4.9371$ and $\omega_F = 0.255$; therefore, adding the flap to the wing seems to lower the flutter speed and to rise slightly the flutter frequency). [Note also that the linear part of the model was also validated considering the test case presented in Edwards et al. (1979, Fig. 5, p. 368): using the input data indicated in the reference, we obtained a dimensionless flutter speed $U_F = V_F/b\omega_\alpha = 3.003$, which coincides with the value given in the referred paper.]

In Fig. 5 the numerical LCO plunge-mode amplitude, $\bar{\xi}$, is given as function of U, in the neighborhood of U_F, for $c_{3\alpha} = -50$, and for $a_h = -0.50$, -0.49, -0.48, -0.47 and -0.46 (note that the different values of a_h correspond to different positions of the elastic center along the chord). Specifically, these LCO amplitudes are computed with the shooting method [see, e.g., Nayfeh and Balachandran (1994)]. It is apparent from Fig. 5 how the shape of the bifurcation diagram changes with a_h; for $a_h \simeq -0.47$, the Hopf bifurcation changes from subcritical into supercritical, and the turning point disappears, as the absolute value of a_h decreases.

It is important to note that the value of the nonlinear coefficient $c_{3\alpha}$ does not affect the speed at which the turning point appears, but it determines only the LCO oscillation amplitudes. This issue is evident in Fig. 6, where the curves for the LCO amplitudes of $\bar{\xi}$, $\bar{\alpha}$ and $\bar{\beta}$ for the case $c_{3\alpha} = -50$ are depicted together with the plunge amplitude for the case $c_{3\alpha} = -40$.

The following comments arise from a first analysis of Figs. 5 and 6 (and similar successive figures) concerning the local study presented, in the neighborhood of the linear stability limit (i.e., when $U \simeq U_F$). The first comment is that the safe flight speed is slightly reduced, i.e., the possible onset of undamped oscillations is anticipated in correspondence of the turning-point abscissa $U_{TP} \simeq 4.674$ with respect to $U_F \simeq 4.677$. Specifically, for $U < U_{TP}$ the steady-state trivial stable solutions are reached starting from any initial conditions; for $U_{TP} \leqslant U \leqslant U_F$, steady-state trivial solutions are reached for sufficiently limited initial conditions (where the limit is essentially given by the unstable branch); finally, for $U > U_F$, a LC solution type is reached for any initial conditions. Therefore, although the range given by $U_{TP} \leqslant U \leqslant U_F$ may appear as not too significant from a practical point of view, this becomes relevant if interpreted as a 'boundary layer' stability region in nonlinear aeroelastic analysis. Indeed, the second related comment is that the steady-state LCO

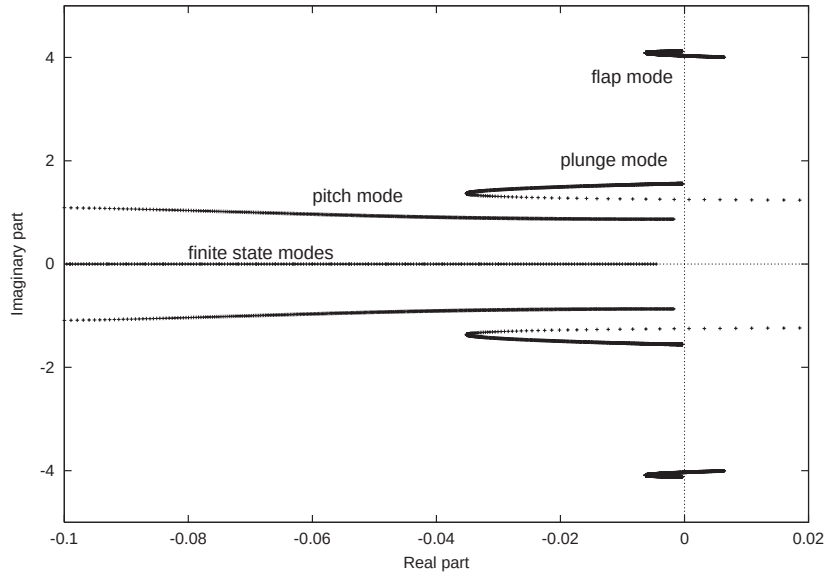

Fig. 4. Root locus for the poles of the linear part of the aeroelastic equations.

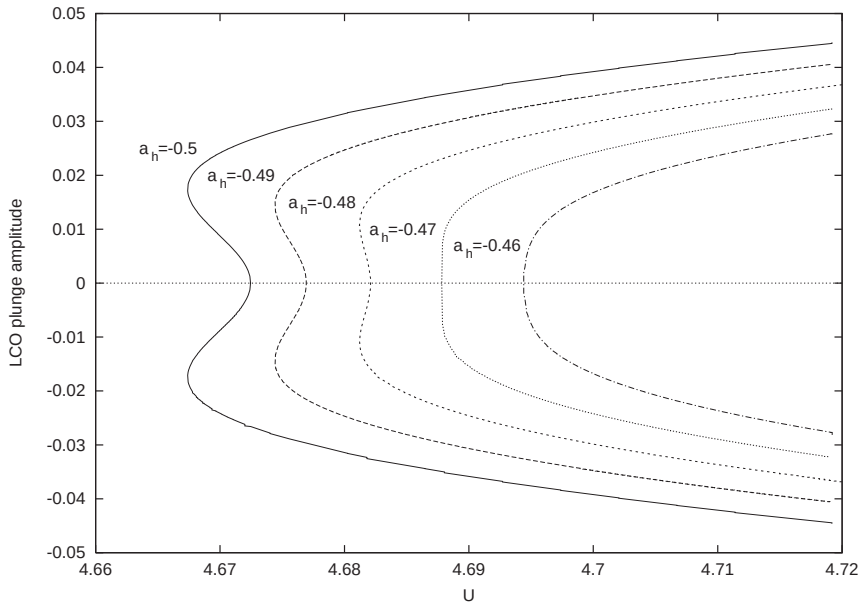

Fig. 5. Pitch NL case: bifurcation plot of the plunge amplitude of LCOs with respect to the nondimensional flight speed U.

amplitudes do not continuously vary with respect to the flight-speed parameter, as there is a stability jump between the trivial steady solutions and the LC solutions if the given initial conditions have sufficiently high values. This issue, together with the previous one, gives as general comment that the nonlinear analysis makes the original stability limit more fuzzy with respect to the linear one, in the sense that the transient from the stable region to the unstable one occurs through the crossing of a thin region as function of the velocity-flow parameter ($U_{TP} \leqslant U \leqslant U_F$) and not of an isolated point as in the linear stability analysis or in the standard bifurcation scenario. This 'boundary layer' stability region, where the most interesting nonlinear pre-critical behaviors occur, has been evaluated in the present analysis.

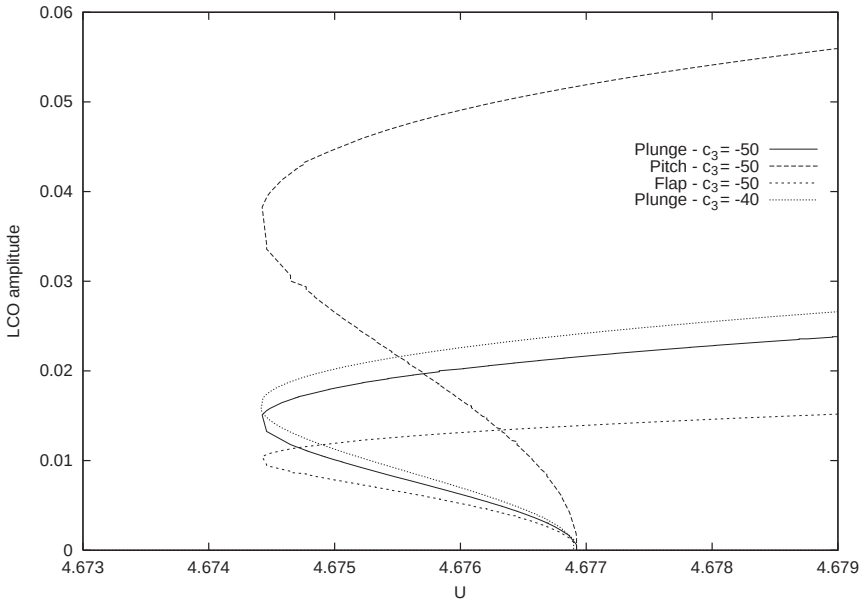

Fig. 6. Pitch NL case: bifurcation plot of the plunge amplitude of LCOs with respect to the nondimensional flight speed U, for $c_{3\alpha} = -50$ and $c_{3\alpha} = -40$ with $a_h = -0.49$.

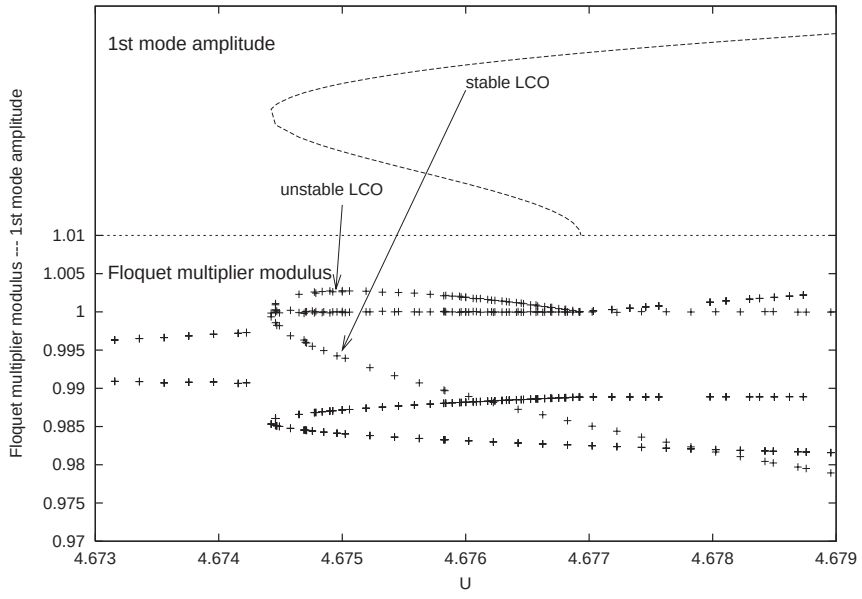

Fig. 7. Pitch NL case: modulus of Floquet multipliers at varying flight speeds.

Next, the stability of these LCOs may be analysed by means of the Floquet theory [see, e.g., Nayfeh and Balachandran (1994)]. The results are shown in Fig. 7, which depicts in the neighborhood of the flutter speed (for $a_h = -0.49$) the modulus of the critical Floquet multipliers both for stable and unstable LC (i.e., those with values close or equal to one; recall that if a Floquet multiplier is outside the unit circle, the corresponding LCO is unstable). As indicated, the upper branch of the first Floquet curve refers to the unstable limit cycle which starts at the bifurcation point (modulus larger than one). On the other hand, the lower branch of this curve refers to the stable limit cycle (into which the unstable one turns at the turning point).

Let us consider the approximate limit-cycle solutions, as obtained with the NF outlined before, and shown in Fig. 8 for the case $a_h = -0.49$. The dotted curves, as obtained by the LC steady solution of the NF method, Eq. (31), corresponds to the fifth (curve on right) and third (curve on left) NF approximation whereas the solid curve corresponds to the direct numerical simulation.

It should be emphasized that the NF curves are obtained using only a pair of complex conjugate equations, which correspond to the critical eigenvalues, whereas the numerical simulation involves the complete system. It is remarkable that the third-order approximation does not capture (not even qualitatively) the 'knee-type' higher-order bifurcations. On the other hand, the fifth-order approximation detects the existence of stability reversal at the turning point, but underestimates both the pre-flutter instability range and the LCO amplitudes. As mentioned above, the discrepancy in the curves is explained later in terms of the inadequacy of the use of two modes (corresponding to the critical eigenvalues) in the fifth-order analysis.

Specifically, in obtaining these results, the NF perturbation technique has been applied under the heuristic assumption (correctly prescribed by the Hopf bifurcation theorem in the case of pitchfork bifurcations) that the modes to be used are those identified by the center-manifold theorem [i.e., the linearly undamped or marginal modes; see, e.g., Guckenheimer and Holmes (1983)]; indeed, the NF approach, whenever applied to the center manifold, can give results only for the space-state variable associated with the first mode. Furthermore, in the case of a fifth-order approximation this assumption leads to uncorrected results because it is clearly violated even for small values of $U - U_F$, since the first two pairs of damped modes become relevant as shown in Fig. 9 whose amplitudes are given by the modulus of the unknown u_3 (or $u_4 \equiv \bar{u}_3$), and the modulus of the unknown u_5 (or $u_6 \equiv \bar{u}_5$, where the overbar indicates the complex conjugate).

This issue implies that, using the perturbation analysis, also the contribution of other complex state variables should be included. This was investigated as shown in Section 3. The $\hat{\lambda}$-points are plotted in Fig. 10 for every combination of $i, j_1, \ldots, j_m$ (each one corresponding to a different nonlinear term), for $U = U_F$. We obtained, by trial and error, that the $\hat{\lambda}$-points inside the curve depicted in Fig. 11 for the case $a_h = -0.49$ are considered as 'near-resonant' (i.e., 'small divisors' in Poincaré's terminology); in other words, this one correspondingly has the minimal set of equations that yields a good agreement between the solution of the NF equations and that of the original equations. Specifically, if we increased the number of $\hat{\lambda}$-points, no difference was observed; on the other hand, if any of the $\hat{\lambda}$-points in the 'minimal set' was removed, substantial deterioration was obtained. It is worth noting that the curve in Fig. 11 is a circle: this fact is used in Fig. 12, where the time history of $\sqrt{u_1 \bar{u}_1}$, is plotted for increasing values of the circle radius ρ (i.e., adding more and more nonlinear terms until a satisfactory solution is obtained). Good agreement with the full-system solution is achieved in this case for $\rho = 0.1$. Note that the same number of nonlinear terms was retained also in the NF

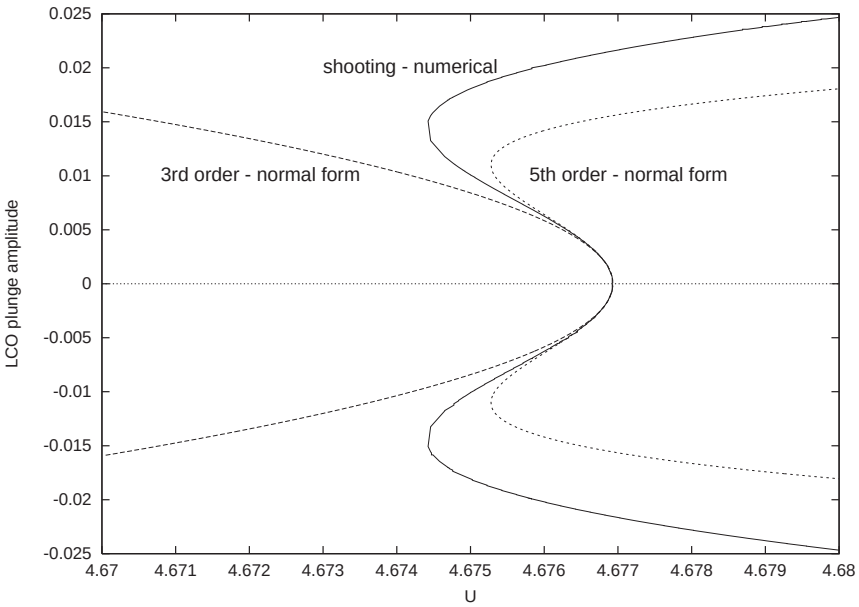

Fig. 8. Pitch NL case: bifurcation plot of the plunge amplitude of LCOs with respect to the nondimensional flight speed U; shooting method versus NF method.

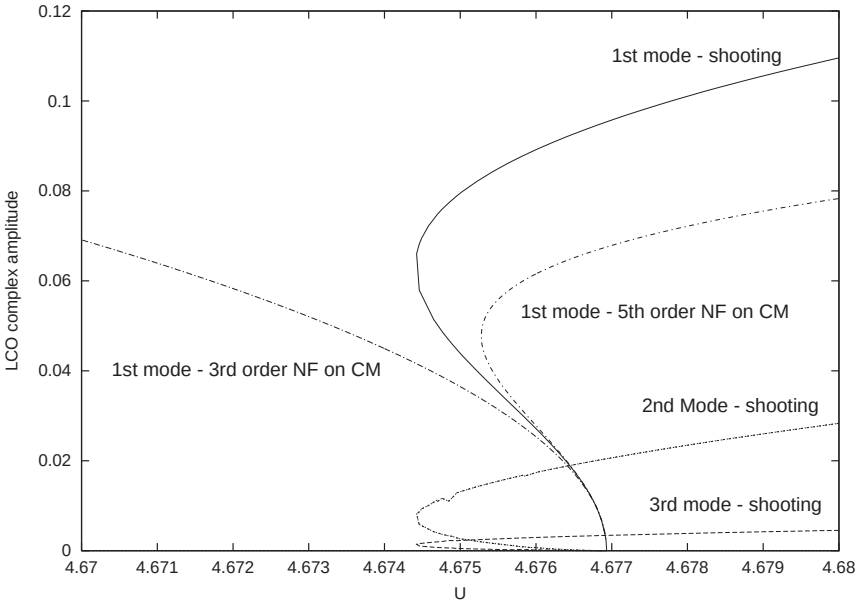

Fig. 9. Pitch NL case: bifurcation plot for $\sqrt{u_1\bar{u}_1}$ and $\sqrt{u_3\bar{u}_3}$ with shooting method and revised NF method.

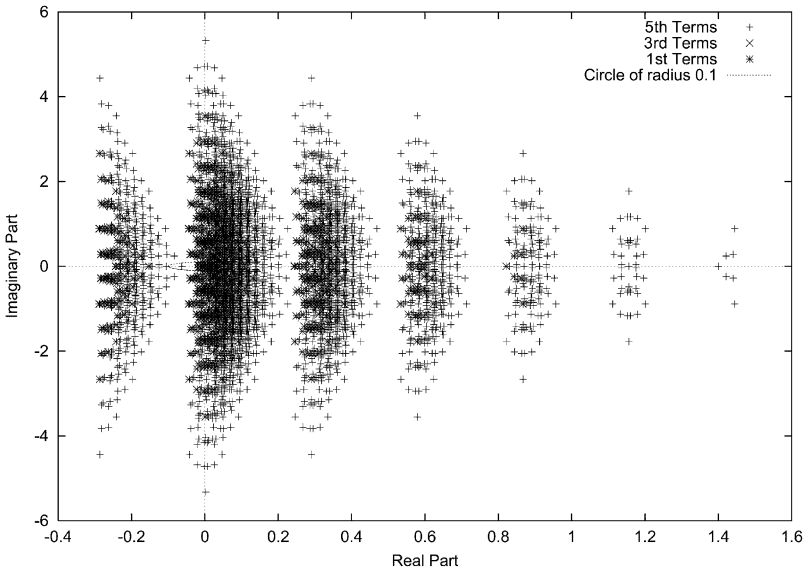

Fig. 10. Pitch NL case: locus of the $\hat{\lambda}$-points.

approximation of Eq. (5) for $U = 4.6724$, which Fig. 12 refers to. This value of ρ is such that no contribution is given by the equations for u_7 and u_8. Thus, the obtained essential equations useful to satisfactorily describe the nonlinear dynamics are

$$\begin{aligned}
\dot{u}_1 &= \lambda_1 u + \sum_{p\in I_p^1} a_{1p}u_p + \sum_{pqr\in I_{pqr}^1} c_{1pqr}u_p u_q u_r + \sum_{pqrst\in I_{pqrst}^1} e_{1pqrst}u_p u_q u_r u_s u_t,\\
\dot{u}_3 &= \lambda_3 u + \sum_{p\in I_p^3} a_{3p}u_p + \sum_{pqr\in I_{pqr}^3} c_{3pqr}u_p u_q u_r + \sum_{pqrst\in I_{pqrst}^3} e_{3pqrst}u_p u_q u_r u_s u_t,\\
\dot{u}_5 &= \lambda_5 u + \sum_{p\in I_p^5} a_{5p}u_p + \sum_{pqr\in I_{pqr}^5} c_{5pqr}u_p u_q u_r + \sum_{pqrst\in I_{pqrst}^5} e_{5pqrst}u_p u_q u_r u_s u_t,
\end{aligned} \tag{39}$$

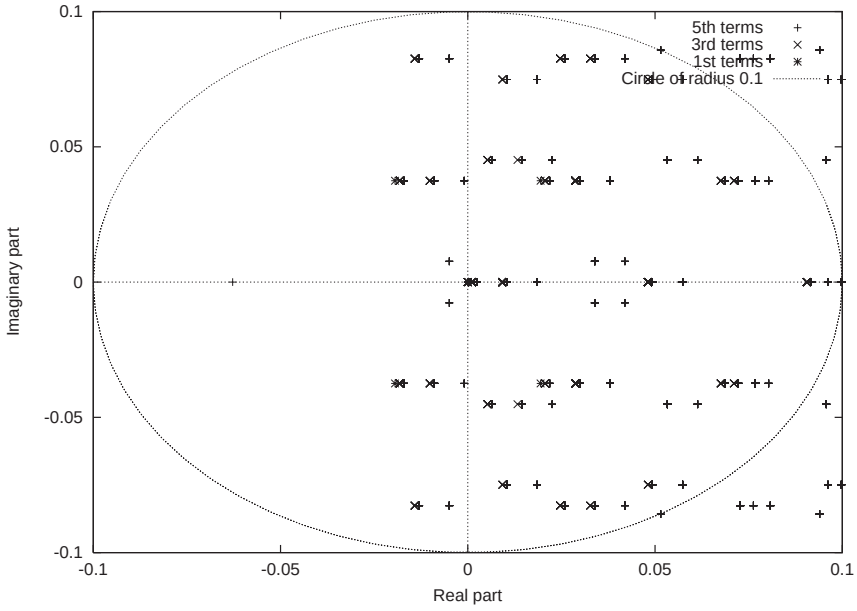

Fig. 11. Pitch NL case: zoom of the locus of the $\hat{\lambda}$-points.

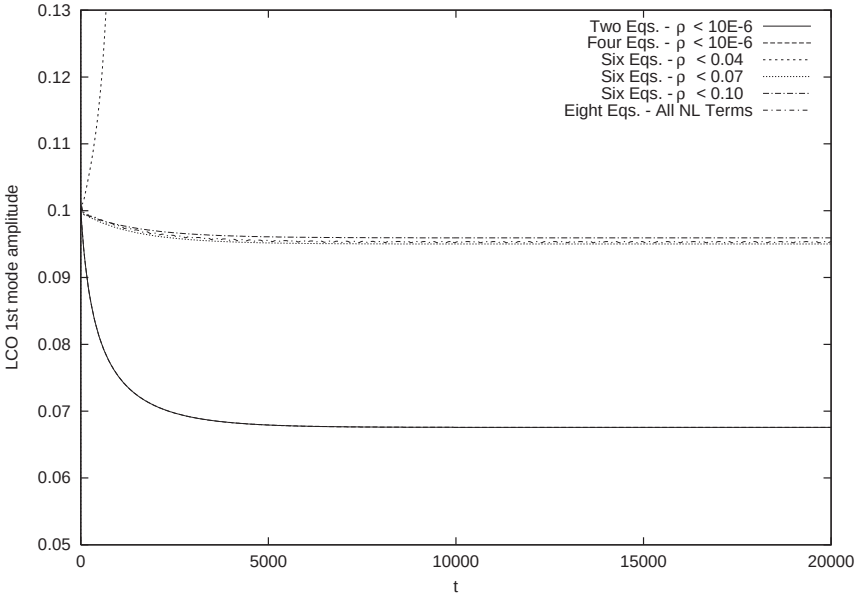

Fig. 12. Pitch NL case: time-history of the generalized coordinates obtained with different NF approximations.

where $u_2 = \bar{u}_1$, $u_4 = \bar{u}_3$ and $u_5 = \bar{u}_6$. The generic index combinations $I_{i,q}$ are such that the corresponding eigenvalues give a $\hat{\lambda}$-point located inside the circle of radius $\rho = 0.1$. A summary of the results is given in Fig. 13, where the absolute value of the LCO amplitudes of u_1 (critical mode), u_3 and u_5 are given for some values of U; the lines refer to numerical integration results (where the shooting method was employed), whereas the points are obtained using the NF including the contribution of the equations associated to the $\hat{\lambda}$-points located inside the circle with radius $\rho = 0.1$. It is worth to point out that all the mode amplitudes—mainly related with the structural dof—are computed by solving Eqs. (39).

In the following part of this section, we assume that $M_\alpha(\alpha) = \alpha$ and $M_\beta(\beta) = c_{1\beta}\beta + c_{3\beta}\beta^3$ (the values of the other typical section coefficients are unchanged). If $c_{1\beta}$ is put equal to one, the same linear flutter speed is obviously obtained

as in the case of the typical section with a nonlinear spring in pitch. In order to make a comparison with the previous nonlinear case, $c_{3\beta} = -50$ is assumed, giving the subcritical (pitchfork) bifurcation shown in Fig. 14. The amplitude of plunge LCOs obtained via the shooting method is indicated with the solid line, whereas with the dashed lines the third- and fifth-order NF approximations of the amplitude of LCOs are depicted. It is clear how the fifth-order approximation of the unstable LCOs is improved with respect to the third order NF form analysis. If the sign of the nonlinearity is reversed ($c_{3\beta} = 50$), the unstable limit cycle is changed into a stable one as shown in Fig. 15 (the same kind of comments about the accuracy of NF approximations can be given again).

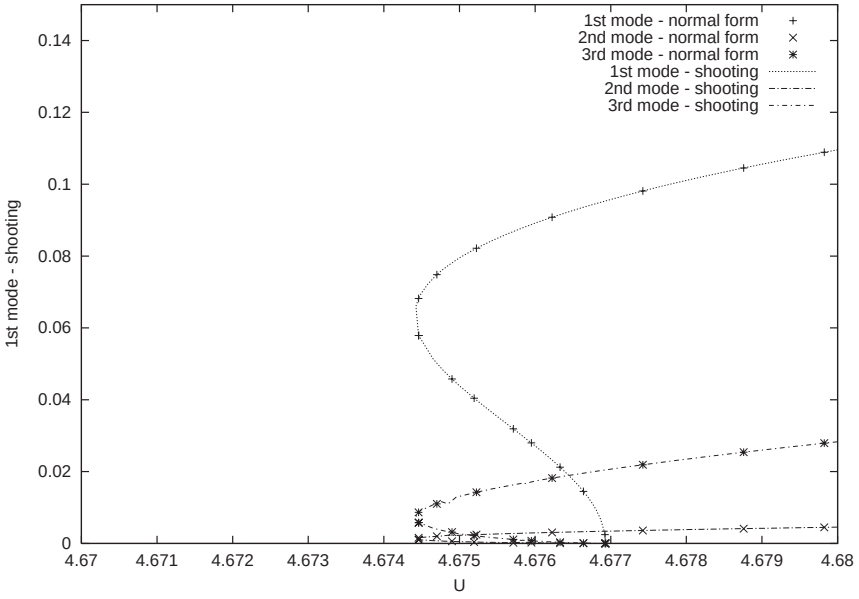

Fig. 13. Pitch NL case: bifurcation plot with respect to the nondimensional flight speed U for different $\hat{\lambda}$-point terms.

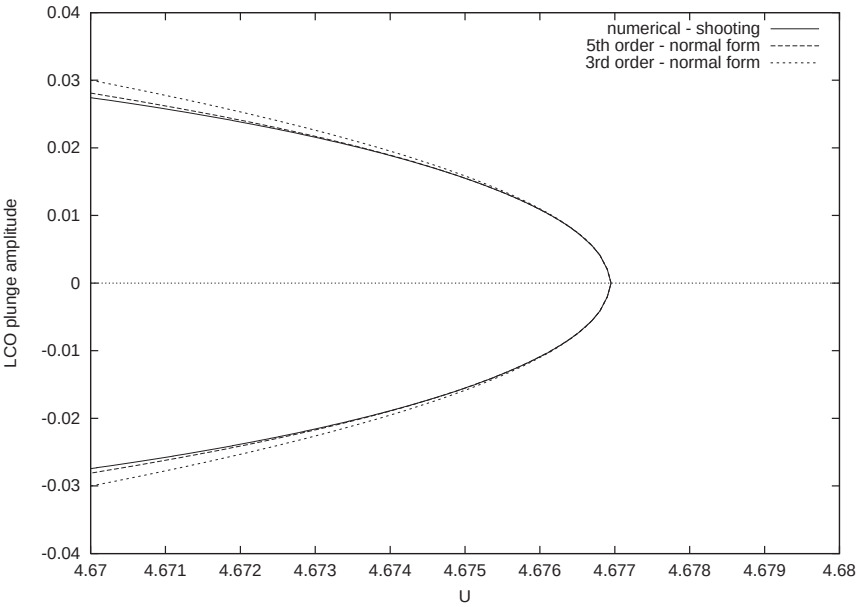

Fig. 14. Flap NL case: bifurcation plot with respect to the nondimensional flight speed U for $c_{1\beta} = 1$ and $c_{3\beta} = -50$: shooting versus NF method.

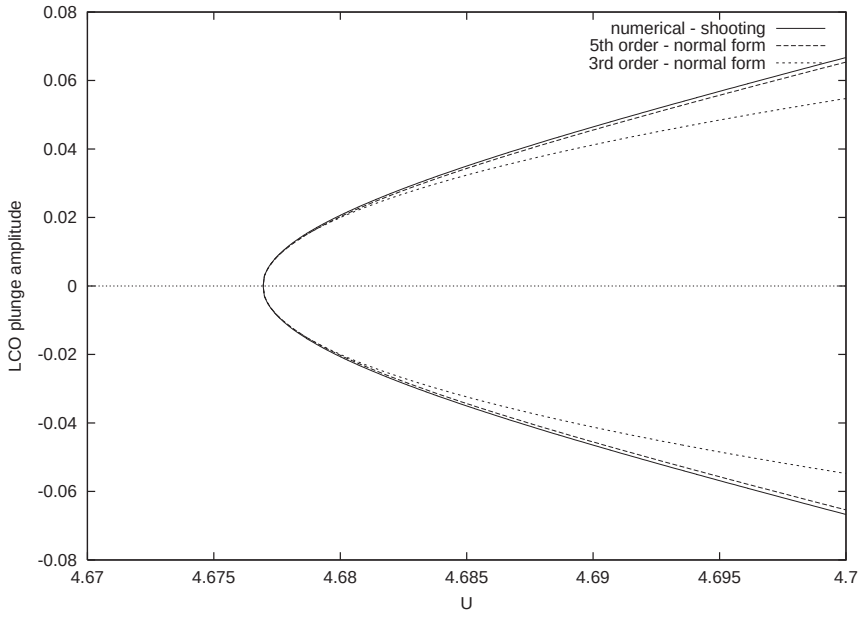

Fig. 15. Flap NL case: bifurcation plot with respect to the nondimensional flight speed U for $c_{1\beta} = 1$ and $c_{3\beta} = 50$: shooting versus NF method.

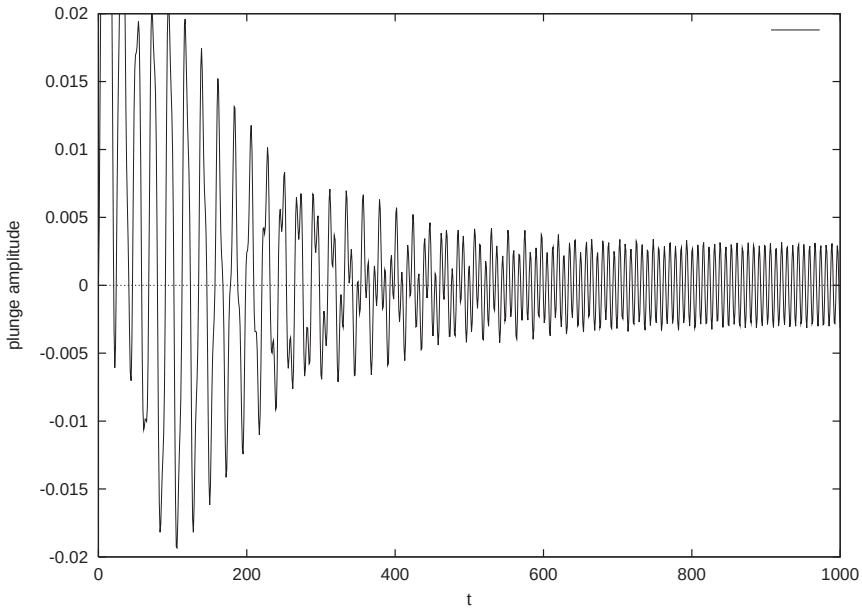

Fig. 16. Flap NL case: time history of plunge for $c_{1\beta} = 0.85$, $c_{3\beta} = 50$ and $U = 4.474$.

A case more similar to that of freeplay in the control surfaces is obtained when $c_{1\beta}$, the linear part of the flap restoring moment, is decreased (in the case of freeplay, the tangent of the curve of the restoring moment at the origin is horizontal). As long as $c_{1\beta}$ is decreased, the flutter speed reduces too. It is interesting also to note that for $c_{1\beta} \simeq 0.85$ the mode that becomes (linearly) unstable is no longer the plunge mode but the flap mode. This causes a significant change in the LCOs, which are greatly reduced; this is strictly related with the derivative of the real part of the critical eigenvalue with respect to U at U_F, which is much smaller for the flap mode than for the plunge mode. In Fig. 16, the time history of plunge is depicted for $U = 4.474 > U_F$. As one can see in the first part of the diagram in Fig. 16 (up to

$t = 180$ dimensionless time), the response to given initial conditions is dominated (because of the initial conditions themselves) by the plunge aeroelastic mode which is not, however, the mode nonlinearly involved in the LCO as clearly shown by the NF analysis. Therefore, after a transient phase which is active up to $t = 800$, the response stabilizes in a LCO having a different frequency which is that of the center manifold [i.e., the imaginary part of the pitch critical aeroelastic pole: it is worth pointing out that, from nonlinear system theory, the eigenspace associated to the critical eigenvalue is the local approximation of the nonlinear concept of "manifold" for small value of parameter perturbation; see, e.g., Guckenheimer and Holmes (1983)].

Finally, it is also worth to note that, for values of $c_{1\beta}$ close to 0.85, the plunge-mode and the flap-mode eigenvalues cross the imaginary axis in a very small range of U, and, therefore, a study of higher manifold bifurcations should be required.

5. Concluding remarks

In the present paper some results about a numerical solution and a semi-analytical perturbation approach—based on the NF method—of a 3-dof aeroelastic system with cubic nonlinearities are shown and discussed. Both torsional and TE-flap nonlinear features are considered in the analysis of the typical section behavior. Indeed, the equations of the described aeroelastic model, in a first-order state-space form, have allowed to apply a third-order and a fifth-order perturbation method to find out a semi-analytical approximation of the numerical bifurcation plots, revealing both a Hopf bifurcation (specifically, an unstable LCO) and a stability reversal behavior (turning point).

The analysis of this nonlinear aeroelastic model showed the dependence of the bifurcation diagram (pure pitchfork or 'knee'-like shape) upon the position of the elastic center.

Moreover, the NF method has been applied as an actual tool useful to identify the nonlinear contributions responsible in the mathematical model of the reversal behavior. The possible extension of this result could be an inverse procedure based on the use of these indications to achieve suggestions on how to modify some system parameters in order to improve the nonlinear flutter performances (LCO and/or reversal behavior) of a wing.

Acknowledgements

This paper has been supported by the Italian *Ministero delle Infrastrutture e dei Trasporti*, Finanziamento progetti di ricerca di Ateneo Anno 2002.

Appendix. Model Coefficients

The aeroelastic equations of motion for nonlinear 3-D typical section with a TE flap can be written as follows:

$$\begin{aligned} &m\ddot{h} + S_\alpha\ddot{\alpha} + S_\beta\ddot{\beta} + k_h h = \mathscr{L},\\ &S_\alpha\ddot{h} + J_\alpha\ddot{\alpha} + (J_\beta + b(b_h - a_h)S_\beta)\ddot{\beta} + k_\alpha M_\alpha(\alpha) = \mathscr{M}_\alpha,\\ &S_\beta\ddot{h} + (J_\beta + b(b_h - a_h)S_\beta)\ddot{\alpha} + J_\beta\ddot{\beta} + k_\beta M_\beta(\beta) = \mathscr{M}_\beta, \end{aligned} \tag{A.1}$$

where the associated coefficients are defined in Table 1. By defining the following undimensional coefficients

$$\begin{aligned} &\xi = h/b, \quad x_\alpha = S_\alpha/mb, \quad x_\beta = S_\beta/mb,\\ &\omega_h^2 = k_h/m, \quad \omega_\alpha^2 = k_\alpha/J_\alpha, \quad \omega_\beta^2 = k_\beta/J_\beta,\\ &r_\alpha^2 = J_\alpha/mb^2, \quad r_\beta^2 = J_\beta/mb^2, \quad \mu = m/\rho\pi b^2, \end{aligned}$$

and by substituting the above relationships into Eq. (A.1), after some algebra we obtain the equations of motion in a undimensional form

$$\begin{aligned} &\ddot{\xi} + x_\alpha\ddot{\alpha} + x_\beta\ddot{\beta} + \omega_h^2\xi = \frac{\mathscr{L}}{mb},\\ &x_\alpha\ddot{\xi} + r_\alpha^2\ddot{\alpha} + (r_\beta^2 + (b_h - a_h)x_\beta)\ddot{\beta} + r_\alpha^2\omega_\alpha^2 M_\alpha(\alpha) = \frac{\mathscr{M}_\alpha}{mb^2},\\ &x_\beta\ddot{\xi} + (r_\beta^2 + (b_h - a_h)x_\beta)\ddot{\alpha} + \ddot{\beta} + r_\beta^2\omega_\beta^2 M_\beta(\beta) = \frac{\mathscr{M}_\beta}{mb^2}. \end{aligned} \tag{A.2}$$

Table 1
Definitions of coefficients in Eq. (A.1)

ρ	Mass of air per unit of volume
m	Mass of the airfoil (mass of the wing per unit of length)
S_α, S_β	Static moments of wing-flap and flap, respectively
J_α, J_β	Moments of inertia of wing-flap and flap, respectively
k_α, k_h	Torsional stiffness of wing and flap, respectively
a_h, b_h	Distances of airfoil elastic center and flap hinge from airfoil mid-chord

Furthermore, let

$$\begin{aligned} &\Omega_1 = \omega_h/\omega_\alpha, \quad \Omega_2 = \omega_\beta/\omega_\alpha, \\ &U = V/b\omega_\alpha, \quad \tau = Vt/b = U\omega_\alpha t, \end{aligned} \tag{A.3}$$

so that the equations of motion become (from now on, the time derivatives are assumed to be performed with respect to τ)

$$\begin{aligned} &\ddot{\xi} + x_\alpha\ddot{\alpha} + x_\beta\ddot{\beta} + \frac{\Omega_1^2}{U^2}\xi = \frac{\mathscr{L}}{mb\omega_\alpha^2U^2}, \\ &\frac{x_\alpha}{r_\alpha^2}\ddot{\xi} + \ddot{\alpha} + [r_\beta^2 + (b_h - a_h)x_\beta]\frac{1}{r_\alpha^2}\ddot{\beta} + \frac{1}{U^2}M_\alpha(\alpha) = \frac{\mathscr{M}_\alpha}{r_\alpha^2mb^2\omega_\alpha^2U^2}, \\ &\frac{x_\beta}{r_\beta^2}\ddot{\xi} + \left[1 + (b_h - a_h)\frac{x_\beta}{r_\beta^2}\right] + \ddot{\beta} + \frac{\Omega_2^2}{U^2}M_\beta(\beta) = \frac{\mathscr{M}_\beta}{r_\beta^2mb^2\omega_\alpha^2U^2}, \end{aligned}$$

where the aerodynamic forces are given by (Theodorsen, 1935, p. 419)

$$\mathscr{L}(\xi,\alpha,\beta) = -\rho U^2b^3\omega_\alpha^2\pi[\dot{\alpha} + \ddot{\xi} - a_h\ddot{\alpha} - (T_4/\pi)\dot{\beta} - (T_1/\pi)\ddot{\beta} - 2\,u(w_{3/4})],$$

$$\begin{aligned} \mathscr{M}_\alpha(\xi,\alpha,\beta) = &-\rho U^2b^4\omega_\alpha^2\pi[\bar{a}_h\dot{\alpha} + (1/8 + a_h^2)\ddot{\alpha} + (T_4/\pi + T_{10}/\pi)\beta \\ &+ (T_1/\pi - T_8/\pi - (b_h - a_h)T_4/\pi + 1/2(T_{11}/\pi))\dot{\beta} \\ &- (T_7/\pi + (b_h - a_h)T_1/\pi)\ddot{\beta} - a_h\ddot{\xi} + 2(a_h + 1/2)\,u(w_{3/4})], \end{aligned}$$

$$\begin{aligned} \mathscr{M}_\beta(\xi,\alpha,\beta) = &-\rho U^2b^4\omega_\alpha^2\pi[(-2T_9/\pi - T_1/\pi - \bar{a}_hT_4/\pi)\dot{\alpha} + 2(T_{13}/\pi)\ddot{\alpha} \\ &+ (T_5 - T_4T_{10})/\pi)\beta - 1/2\,(T_4T_{11}/\pi)\,\dot{\beta} - (T_3/\pi)\ddot{\beta} \\ &- (T_1/\pi)\ddot{\xi} - (T_{12}/\pi)u(w_{3/4})]. \end{aligned} \tag{A.4}$$

Substituting the expression of the forces into the equation of motion, one obtains

$$\begin{aligned} &\ddot{\xi} + x_\alpha\ddot{\alpha} + x_\beta\ddot{\beta} + \frac{\Omega_1^2}{U^2}\xi = p, \\ &\frac{x_\alpha}{r_\alpha^2}\ddot{\xi} + \ddot{\alpha} + [r_\beta^2 + (b_h - a_h)x_\beta]\frac{1}{r_\alpha^2}\ddot{\beta} + \frac{1}{U^2}M_\alpha(\alpha) = r, \\ &\frac{x_\beta}{r_\beta^2}\ddot{\xi} + \left[1 + (b_h - a_h)\frac{x_\beta}{r_\beta^2}\right]\ddot{\alpha} + \ddot{\beta} + \frac{\Omega_2^2}{U^2}M_\beta(\beta) = s, \end{aligned} \tag{A.5}$$

where

$$p \coloneqq \frac{-1}{\mu}\frac{\mathscr{L}(\xi,\alpha,\beta)}{\rho U^2b^3\omega_\alpha^2\pi}, \quad r \coloneqq \frac{-1}{\mu r_\alpha^2}\frac{\mathscr{M}_\alpha(\xi,\alpha,\beta)}{\rho U^2b^4\omega_\alpha^2\pi}, \quad s \coloneqq \frac{-1}{\mu r_\beta^2}\frac{\mathscr{M}_\beta(\xi,\alpha,\beta)}{\rho U^2b^4\omega_\alpha^2\pi}.$$

By multiplying the second and the third equation for r_α^2 and r_β^2, respectively, it follows that

$$\begin{aligned}
&\ddot{\xi} + x_\alpha \ddot{\alpha} + x_\beta \ddot{\beta} + \frac{\Omega_1^2}{U^2}\xi = p,\\
&x_\alpha \ddot{\xi} + r_\alpha^2 \ddot{\alpha} + [r_\beta^2 + (b_h - a_h)x_\beta]\ddot{\beta} + \frac{r_\alpha^2}{U^2} M_\alpha(\alpha) = r_\alpha^2 r,\\
&x_\beta \ddot{\xi} + [r_\beta^2 + (b_h - a_h)x_\beta]\ddot{\alpha} + r_\beta^2 \ddot{\beta} + \frac{r_\beta^2 \Omega_2^2}{U^2} M_\beta(\beta) = r_\beta^2 s.
\end{aligned} \tag{A.6}$$

The equation of motion can be re-written in the case of presence of cubic nonlinearities only, in the following second-order matrix form:

$$(\mu \mathbf{M}_s + \mathbf{M}_{nc})\ddot{\mathbf{x}} + \mathbf{C}_{nc}\dot{\mathbf{x}} + (\mu \mathbf{K}_s + \mathbf{K}_{nc})\mathbf{x} + \mu \mathbf{k}_{nl}(\mathbf{x}) = -\mathbf{r}_c u(w_{3/4}), \tag{A.7}$$

where [see Theodorsen (1935), for the definition of T_i's for $i = 1, 2, \ldots, 11$]

$$\mu \mathbf{M}_s + \mathbf{M}_{nc} = \mu \begin{bmatrix} 1 & x_\alpha & x_\beta \\ x_\alpha & r_\alpha^2 & \hat{r}_\beta^2 \\ x_\beta & \hat{r}_\beta^2 & r_\beta^2 \end{bmatrix} + \begin{bmatrix} 1 & -a_h & -T_1/\pi \\ -a_h & 1/8 + a_h^2 & T_{12}/\pi \\ -T_1/\pi & T_{12}/\pi & -T_3/\pi \end{bmatrix}$$

with $\hat{r}_\beta^2 = r_\beta^2 + (b_h - a_h)x_\beta$ and $T_{12}/\pi = -T_7/\pi - (b_h - a_h)T_1/\pi$;

$$\mathbf{C}_{nc} = \begin{bmatrix} 0 & 1 & -T_4/\pi \\ 0 & \bar{a}_h & T_{13} \\ 0 & (-2T_9 - T_1 - \bar{a}_h T_4)/\pi & -1/2 T_4 T_{11}/\pi^2 \end{bmatrix},$$

with $T_{13} = (T_1 - T_8 - (b_h - a_h)T_4 + 1/2 T_{11})/\pi)$. Finally, assuming the presence of nonlinearities of cubic type, or $M_\alpha = c_{1\alpha}\alpha + c_{3\alpha}\alpha^3$ and $M_\beta = c_{1\beta}\beta + c_{3\beta}\beta^3$, one has

$$\begin{aligned}
&\mu \mathbf{K}_s + \mathbf{K}_{nc} = \mu \begin{bmatrix} \dfrac{\Omega_1^2}{U^2} & 0 & 0 \\ 0 & c_{1\alpha}\dfrac{r_\alpha^2}{U^2} & 0 \\ 0 & 0 & c_{1\beta}\dfrac{r_\beta^2 \Omega_2^2}{U^2} \end{bmatrix} + \begin{bmatrix} 0 & 0 & 0 \\ 0 & 0 & (T_4 + T_{10})/\pi \\ 0 & 0 & (T_5 - T_4 T_{10})/\pi^2 \end{bmatrix},\\
&\mu \mathbf{k}_{nl}(\mathbf{x}) = \mu \left\{ 0, \quad c_{3\alpha}\frac{r_\alpha^2}{U^2}\alpha^3, \quad c_{3\beta}\frac{r_\beta^2 \Omega_2^2}{U^2}\beta^3 \right\}^{\mathrm{T}}
\end{aligned} \tag{A.8}$$

and

$$\mathbf{r}_c = \{-2, \quad +2(1/2 + a_h), \quad -T_{12}/\pi\}^{\mathrm{T}}. \tag{A.9}$$

References

Alighanbari, H., Lee, B.H.K., 2003. Analysis of nonlinear aeroelastic signals. Journal of Aircraft 40, 552–558.

Alighanbari, H., Price, S.J., 1996. The post-Hopf bifurcation response of an airfoil in incompressible two-dimensional flow. Nonlinear Dynamics 10, 381–400.

Chen, P.C., Sarhaddi, D., Liu, D.D., 1998. Limit-cycle-oscillations studies of a fighter with external stores. AIAA Conference Paper with Number: AIAA-98-1727, pp. 258–266.

Conner, M.D., Tang, D.M., Dowell, E.H., Virgin, L.N., 1997. Nonlinear behavior of a typical airfoil section with control surface with freeplay: a numerical and experimental study. Journal of Fluids and Structures 11, 89–109.

Dessi, D., Mastroddi, F., Morino, L., 2002. Limit-cycle stability reversal near a Hopf bifurcation with aeroelastic applications. Journal of Sound and Vibration 256, 347–365.

Dowell, E.H., Virgin, L.N., Tang, D.M., Conner, M.D., 1997. Nonlinear dynamics of aeroelastic systems. Proceedings of International Forum on Aeroelasticity and Structural Dynamics, Rome, Italy, 17–20 June, pp. 79–91.

Edwards, J.W., Ashley, H., Breakwell, J.V., 1979. Unsteady aerodynamic modelling for arbitrary motions. AIAA Journal 17, 365–374.

Fung, Y.C., 1955. An Introduction to the Theory of Aeroelasticity. Wiley, New York (reprinted by Dover, New York, 1969).

Guckenheimer, J., Holmes, P., 1983. Nonlinear Oscillations, Dynamical Systems, and Bifurcations of Vector Field. Springer, New York.

Jones, R.T., 1940. The unsteady lift of a wing of finite aspect ratio. NACA Report 681.

Lacabanne, M., 1997. An experimental analysis of the aeroelastic behaviour with a freeplay in a control surface. Proceedings of International Forum on Aeroelasticity and Structural Dynamics, Rome, Italy, 17–20 June, pp. 79–91.

Lee, B.H.K, Gong, L., Wong, Y.S., 1997. Analysis and computation of nonlinear dynamic response of a two-degree-of-freedom system and its application in aeroelasticity. Journal of Fluids and Structures 11, 225–246.

Lee, B.H.K., Jiang, L., Wong, Y.S., 1998. Flutter of an airfoil with a cubic nonlinear restoring force. AIAA conference paper with number: AIAA-98-1725.

Lee, B.H.K., Tron, A., 1989. Effects of structural nonlinearities on flutter characteristics of the CF-18 aircraft. Journal of Aircraft 26, 781–786.

Mastroddi, F., Bettoli, A., 1999. Wavelet analysis for Hopf bifurcations with aeroelastic applications. Journal of Sound and Vibration 225, 887–913.

Matsushita, H., Mosekilde, E., Christiansen, L.E., Lehn-Schioler, T.L., Granasy, P., 2001. Examination of the two-degrees-of-freedom nonlinear math model for transonic flutter. Proceedings of International Forum on Aeroelasticity and Structural Dynamics, Madrid, 5–7 June, pp. 287–294.

Morino, L., Mastroddi, F., De Troia, R., Ghiringhelli, G.L., Mantegazza, P., 1995. Matrix fraction approach for finite-state aerodynamic modelling. AIAA Journal 33, 703–711.

Nayfeh, A.H., Balachandran, B., 1994. Applied Nonlinear Dynamics. Wiley, New York.

Theodorsen, T., 1935. General theory of aerodynamic instability and the mechanism of flutter. NACA Report 496, pp. 413–433.

Woolston, D.S., Runyan, H.L., Andrews, R.E., 1957. An investigation of certain types of structural nonlinearities on wing and control surface flutter. Journal of Aeronautical Sciences 24, 57–63.